Eur. Phys. J. C 20, 301–311 (2001)
Digital Object Identifier (DOI) 10.1007/s100520100648

THE EUROPEAN PHYSICAL JOURNAL C

On the behavior of F_2 and its logarithmic slopes

A.B. Kaidalov[1,a], C. Merino[2,b], D. Pertermann[3,c]

[1] ITEP, B. Cheremushkinskaya 25, 117259 Moscow, Russia
[2] Departamento de Física de Partículas, Universidade de Santiago de Compostela, 15706 Santiago de Compostela, Spain
[3] Physics Department, University-GH-Siegen, 57068 Siegen, Germany

Received: 12 May 2000 / Revised version: 5 February 2001 /
Published online: 11 May 2001 –

Abstract. It is shown that the CKMT model for the nucleon structure function F_2, taken as the initial condition for the NLO evolution equations in perturbative QCD, provides a good description of the HERA data when presented in the form of the logarithmic slopes of F_2 versus x and Q^2 (Caldwell plot), in the whole available kinematic ranges. Also the results obtained for the behavior of the gluon component of a nucleon are presented.

1 The CKMT model

The CKMT model [1] for the parameterization of the nucleon structure function F_2 is a theoretical model based on Regge theory which provides a consistent formulation of this function in the region of low Q^2 and describes the experimental data on F_2 in that region.

The CKMT model [1] proposes for the nucleon structure functions,

$$F_2(x,Q^2) = F_{\rm S}(x,Q^2) + F_{\rm NS}(x,Q^2), \tag{1}$$

the following parameterization of its two terms in the region of small and moderate Q^2. For the singlet term, corresponding to the pomeron contribution:

$$F_{\rm S}(x,Q^2) = A\cdot x^{-\Delta(Q^2)}\cdot(1-x)^{n(Q^2)+4}\cdot\left(\frac{Q^2}{Q^2+a}\right)^{1+\Delta(Q^2)}, \tag{2}$$

where the $x\to 0$ behavior is determined by an effective intercept of the pomeron, Δ, which takes into account pomeron cuts and, therefore (and this is one of the main points of the model), it depends on Q^2. This dependence was parameterized [1] as

$$\Delta(Q^2) = \Delta_0\cdot\left(1+\frac{\Delta_1\cdot Q^2}{Q^2+\Delta_2}\right). \tag{3}$$

Thus, for low values of Q^2 (large cuts), Δ is close to the effective value found from analysis of the hadronic total cross-sections ($\Delta\sim 0.08$), while for high values of Q^2 (small cuts), Δ takes the bare pomeron value, $\Delta\sim 0.2$–0.25. The parameterization for the non-singlet term, which corresponds to the secondary reggeon (f, A_2) contribution, is

$$F_{\rm NS}(x,Q^2) = B\cdot x^{1-\alpha_{\rm R}}\cdot(1-x)^{n(Q^2)}\cdot\left(\frac{Q^2}{Q^2+b}\right)^{\alpha_{\rm R}}, \tag{4}$$

where the $x\to 0$ behavior is determined by the secondary reggeon intercept $\alpha_{\rm R}$, which is in the range $\alpha_{\rm R}=0.4$–0.5. The valence quark contribution can be separated into the contribution of the u (B_u) and d (B_d) valence quarks, the normalization condition for valence quarks fixes both contributions at one given value of Q^2 (we use $Q^2_{\rm v}=2\,{\rm GeV}^2$ in our calculations). For both the singlet and the non-singlet terms, the behavior when $x\to 1$ is controlled by $n(Q^2)$, where $n(Q^2)$ is

$$n(Q^2) = \frac{3}{2}\cdot\left(1+\frac{Q^2}{Q^2+c}\right). \tag{5}$$

Therefore, for $Q^2=0$ the valence quark distributions have the same power, given by Regge intercepts, as in the quark gluon string model [2] or in the dual parton model [3], $n(0)=\alpha_{\rm R}(0)-\alpha_{\rm N}(0)\sim 3/2$, while the behavior of $n(Q^2)$ for large Q^2 is taken to coincide with dimensional counting rules.

The total cross-section for real ($Q^2=0$) photons can be obtained from the structure function F_2 using the following relation:

$$\sigma^{\rm tot}_{\gamma p}(\nu) = \left[\frac{4\pi^2\alpha_{\rm EM}}{Q^2}\cdot F_2(x,Q^2)\right]_{Q^2=0}. \tag{6}$$

The proper $F_2(x,Q^2)\sim Q^2$ behavior when $Q^2\to 0$ is given in the model by the last factors in (2) and (4), leading to the following form of the $\sigma^{\rm tot}_{\gamma p}(\nu)$ in the CKMT model:

[a] e-mail: kaidalov@vxitep.itep.ru
[b] e-mail: merino@fpaxp1.usc.es
[c] e-mail: pertermann@physik.uni-siegen.de

Table 1. Values of the parameters in the CKMT model obtained in the fit of F_2 when also the low Q^2 HERA data are included. All dimensional parameters are given in GeV^2. The valence counting rules provide the following values of B_u and B_d, for the proton case, when fixing their normalization at $Q^2_{\mathrm{v}} = 2\,\mathrm{GeV}^2$: $B_u = 1.1555$, $B_d = 0.1722$

CKMT model	Values of the parameters
A	0.1301
a	0.2628
Δ_0	0.09663
Δ_1	1.9533
Δ_2	1.1606
c	3.5489 (fixed)
b	0.3840
α_{R}	0.4150 (fixed)

$$\sigma^{\mathrm{tot}}_{\gamma p}(\nu) = 4\pi^2\alpha_{\mathrm{EM}} \cdot \left(A \cdot a^{-1-\Delta_0} \cdot (2m\nu)^{\Delta_0} + (B_u + B_d) \cdot b^{-\alpha_{\mathrm{R}}} \cdot (2m\nu)^{\alpha_{\mathrm{R}}-1}\right). \quad (7)$$

The parameters in the model were determined [1] from a joint fit of the $\sigma^{\mathrm{tot}}_{\gamma p}$ data and the NMC data [4] on the proton structure function in the region $1\,\mathrm{GeV}^2 \leq Q^2 \leq 5\,\mathrm{GeV}^2$, obtaining a very good description of the available experimental data.

The next step in this approach is to introduce the QCD evolution in the partonic distributions of the CKMT model and thus to determine the structure functions at higher values of Q^2. For this, the evolution equation in two loops in the $\overline{\mathrm{MS}}$ scheme with $\Lambda = 200\,\mathrm{MeV}$ was used [1].

The results obtained by taking into account the QCD evolution in this way are [1] in a very good agreement with the experimental data on $F_2(x, Q^2)$ at high values of Q^2.

The HERA data [5,6] on F_2 at low and moderate Q^2 provided the opportunity of including in the fit experimental points from the kinematical region where the CKMT parameterization should give a good description without any QCD evolution. Thus, we added [7] these new H1 and ZEUS data on F_2 at low and moderate Q^2 to those from the NMC [4] and E665 [8] collaborations, and to the data [9] on cross-sections for real photoproduction, to obtain a global fit which allowed for the test of the model in wider regions of x and Q^2. For this new fit, one took as initial conditions for the values of the different parameters those obtained in the previous fit [1], and although the quality of the fit is not very sensitive to small changes in the values of the parameters, the best fit has been found for the values of the parameters given in Table 1.

The quality of the description provided by the CKMT model of all the experimental data on $\sigma^{\mathrm{tot}}_{\gamma p}$ and F_2, and, in particular, of the new experimental data from HERA, is very high (χ^2/d.o.f. $= 106.95/167$ for the global fit, with the statistical and systematic errors treated in quadrature, and the relative normalization among all the experimental data sets taken equal to 1).

Thus, the general features of the CKMT model describe the experimental data in the region of low Q^2 ($0 < Q^2 < Q^2_0$), and therefore this parameterization can be taken at a starting value of Q^2, Q^2_0, as the initial condition in the NLO QCD evolution equation, to obtain F_2 at values of Q^2 higher than Q^2_0. In order to determine the distributions of gluons in a nucleon, the CKMT model assumes [1] that the sea-quark and gluon distributions are different only in the region $x \to 1$. Following [10] we have

$$xg(x, Q^2) = Gx\bar{q}(x, Q^2)/(1 - x), \quad (8)$$

where $x\bar{q}(x, Q^2)$ is proportional to the expression in (2). The constant G is determined from the energy-momentum conservation sum rule.

This approach provides a smooth transition from the region of small Q^2, which is governed by the physics of Regge theory, to a region of large Q^2, where the effects of QCD evolution are important. We have performed our calculations for the two different values of $Q^2_0 = 2\,\mathrm{GeV}^2$ and $Q^2_0 = 4\,\mathrm{GeV}^2$. We also show our results in the shape of both the $\mathrm{d}F_2/\mathrm{d}\ln Q^2$ and the $\mathrm{d}\ln F_2/\mathrm{d}\ln(1/x)$ slopes in order to compare with the experimental data when these are given in the so-called Caldwell plot.

The Q^2 dependence of F_2 can be summarized as follows (see Appendix A for the technical details in the calculation of the NLO QCD evolution of F_2 and its logarithmic derivatives $\mathrm{d}F_2/\mathrm{d}\ln Q^2$, and $\mathrm{d}\ln F_2/\mathrm{d}\ln(1/x)$):

(1) In the region $0 < Q^2 \leq Q^2_0$ we use the pure CKMT model for F_2, (1)–(5).
(2) For $Q^2_0 < Q^2 \leq Q^2_c$ (charm threshold) [11], one has to consider the QCD evolution of F_2 at NLO in the $\overline{\mathrm{MS}}$ scheme, (13), for a number of flavors $n_f = 3$ (u, d, s). We take as the starting parameterization the one given by the CKMT model. We have used two different values of Q^2_0: $Q^2_0 = 2\,\mathrm{GeV}^2$, and $Q^2_0 = 4\,\mathrm{GeV}^2$.
(3) For $Q^2 > Q^2_c$, the QCD evolution is computed at NLO in the $\overline{\mathrm{MS}}$ scheme, but now with a number of flavors $n_f = 4$, and by using the parton distribution functions for the u, d, s, and c quarks. The charm is produced as massless quark in the evolution process.

The charm production is of particular interest. Following [11,12], the assumption of a massless charm quark produced above the threshold $Q^2_c = 4m^2_c$ (m^2_c being the charm quark mass) via the usual DGLAP evolution is not realistic. This procedure is useful in the range of high values, $Q^2 \gg Q^2_c$, only. In the intermediate region $Q^2_c < Q^2 < \bar{Q}^2 = 50\,\mathrm{GeV}^2$, the charm can be treated via a photon–gluon fusion process. The corresponding contribution to the structure function is defined as

$$\frac{1}{x}F^c_2(x, Q^2, m^2_c) = 2e^2_c \frac{\alpha_{\mathrm{s}}(\mu^2)}{2\pi} \int_{ax}^{1} \frac{\mathrm{d}y}{y} \cdot C^c_{g,2}\left(\frac{x}{y}, \frac{m^2_c}{Q^2}\right) \cdot g(y, \mu^2), \quad (9)$$

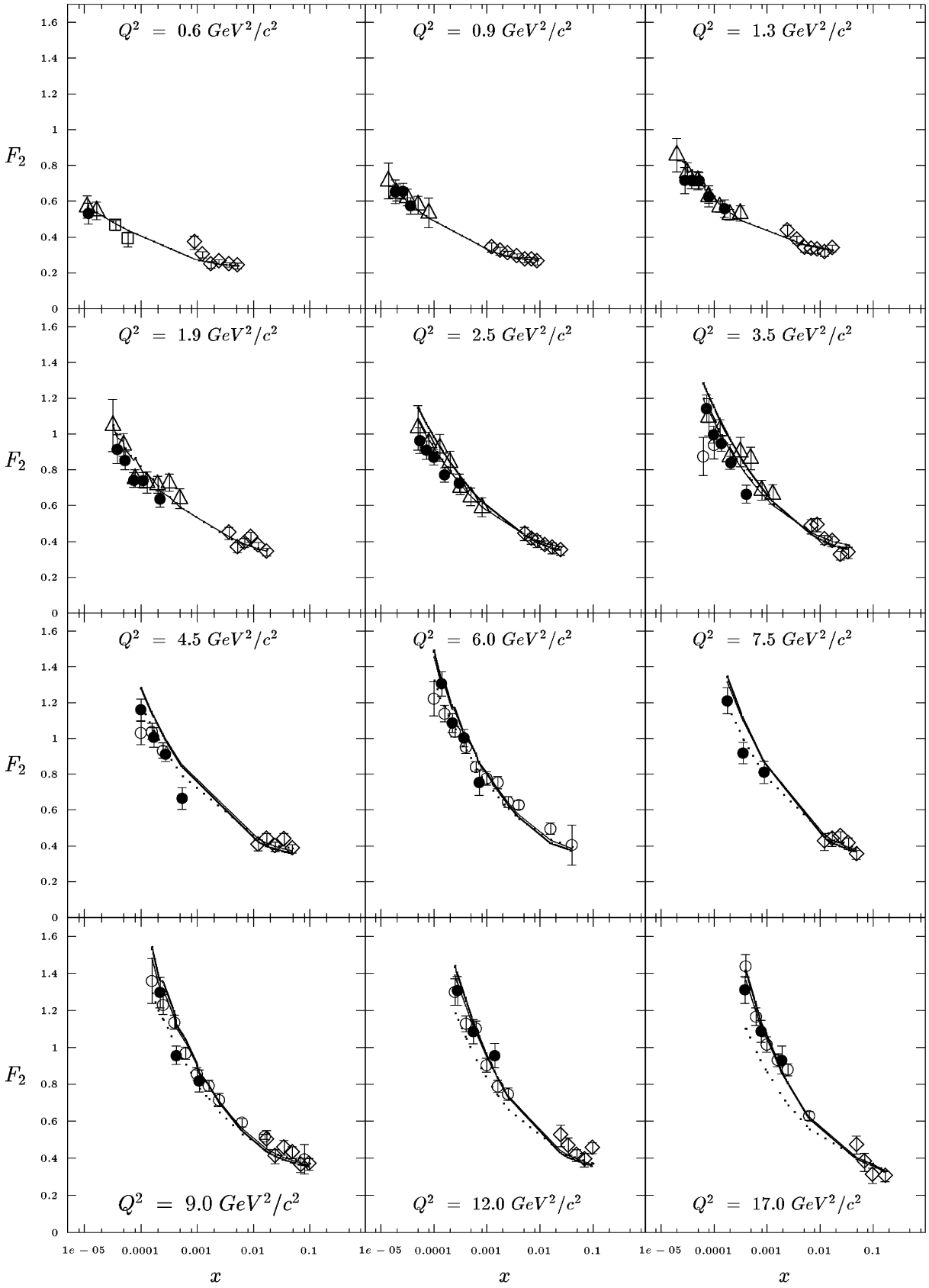

Fig. 1. F_2 as a function of x computed in the CKMT model for twelve different values of Q^2, and compared with the following experimental data (see [14] for the experimental references): ZEUS SVX95 (black circles), H1 SVX95 (white triangles), ZEUS BPC95 (white squares), E665 (white diamonds), and ZEUS 94 (white circles). The dotted line is the theoretical result obtained with the pure CKMT model, and the bold (solid) line is the result obtained with the NLO QCD-evoluted CKMT model when one takes $Q_0^2 = 2\,\mathrm{GeV}^2$ ($Q_0^2 = 4\,\mathrm{GeV}^2$). The bold and solid lines overlap on large regions of x for most of the Q^2 values presented in this figure

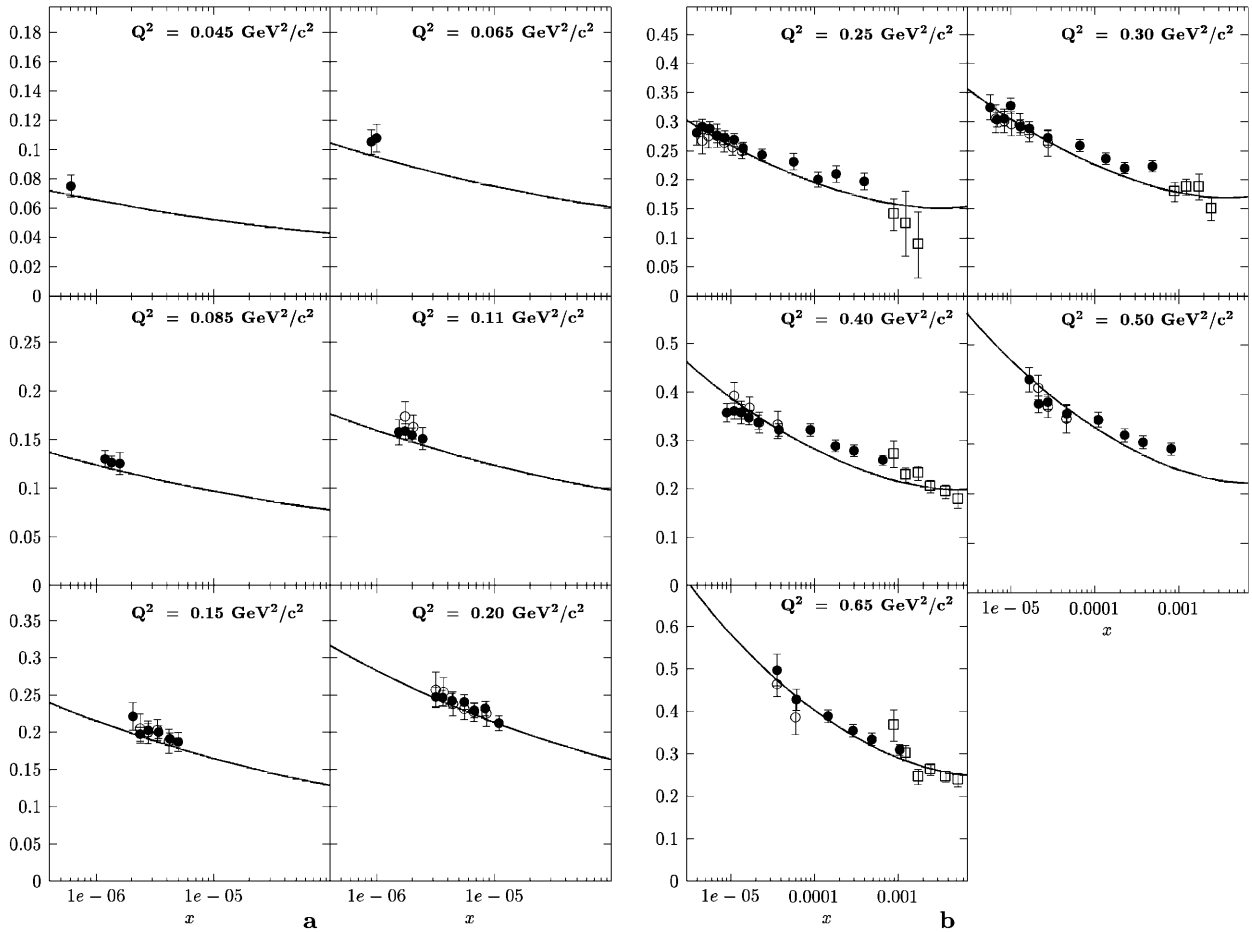

Fig. 2a,b. F_2 as a function of x computed in the CKMT model for six **a** and five **b** different low values of Q^2, and compared with the following experimental data (see [14–16] for the experimental references): ZEUS BPT97 (black circles), ZEUS BPC95 (white circles), and E665 (white squares). The theoretical result has been obtained with the pure CKMT model

where $\mu^2 = 4m_c^2$, $a = 1 + 4m_c^2/Q^2$ and the coefficient $C^c_{g,2}(Z,R)$ is given by

$$C^c_{g,2}(Z,R) = \frac{1}{2}\Bigg\{[Z^2+(1-Z)^2 + 4ZR(1-3Z) - 8Z^2R^2]\ln\frac{1+V}{1-V} + V[-1+8Z(1-Z)-4ZR(1-Z)]\Bigg\}, \quad (10)$$

with $V^2 = 1 - 4RZ/(1-Z)$. So, F_2 is given by (13) in Appendix A, where the sum runs over $q = u, d, s$, plus (9). The contributions of the botom and top quarks are neglected here. The charm threshold is defined as [11,12]

$$W^2 \equiv Q^2(1/x - 1) \geq Q_c^2 = 4m_c^2. \quad (11)$$

The threshold $\bar{Q}^2$ where the charm production in the evolution process becomes more important than the photon–gluon fusion is discussed in detail in [12]. The value $\bar{Q}^2 = 50\,\mathrm{GeV}^2$ is chosen by looking for the smoothness of the transition. This method working better for $x \to 0$ than for $x \to 1$, this explains the small wiggles in some of the figures at $Q^2 = 50\,\mathrm{GeV}^2$.

2 Results

Our results are presented in Figs. 1 to 9.

Figure 1 shows $F_2(x, Q^2)$ as a function of x for several values of Q^2, from $Q^2 = 0.6\,\mathrm{GeV}^2$ to $Q^2 = 17\,\mathrm{GeV}^2$. The dotted lines correspond to the pure CKMT model without any perturbative evolution, while the full lines run for the evoluted CKMT parameterization. When for a given value of Q^2 two full lines are depicted, the bold (solid) one has been obtained by taking the starting point for the QCD evolution as $Q_0^2 = 2\,\mathrm{GeV}^2$ ($Q_0^2 = 4\,\mathrm{GeV}^2$). Experimental points in this figure are from E665 [8], H1 [13], and ZEUS [14] collaborations.

In Figs. 2a,b we present the comparison of the pure CKMT parameterization of F_2 with the low Q^2 data of E665, ZEUS-BPC95, and ZEUS-BPT97, as compiled in [15] and [16]. One sees that the agreement between the CKMT model and the experimental data in this region of low Q^2 is good.

In Fig. 3 (Caldwell plot), the slope $\mathrm{d}F_2/\mathrm{d}\ln Q^2$ is shown as a function of x, and compared with the $a+b\ln Q^2$ fit to the ZEUS F_2 data in bins of x. This plot was considered as evidence for a transition from the hard to the soft regime of QCD in the region of $Q^2 \sim 5\,\mathrm{GeV}^2$ (see

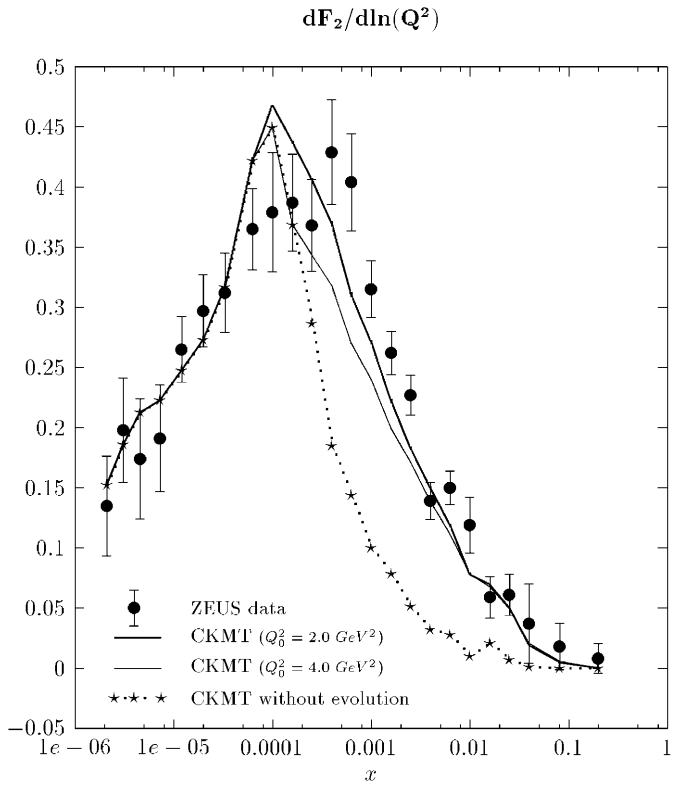

Fig. 3. $\mathrm{d}F_2/\mathrm{d}\ln Q^2$ as a function of x computed by performing the NLO QCD perturbative evolution of the CKMT model (see Appendices A and B for details on the calculation), and compared with the fit to the form $a + b\ln Q^2$ of the ZEUS F_2 data in bins of x (see [14] and references therein for more details on the data and the experimental fit). The dotted line is the theoretical result obtained with the pure CKMT model, and the bold (solid) line is the result obtained with the NLO QCD-evoluted CKMT model when one takes $Q_0^2 = 2\,\mathrm{GeV}^2$ ($Q_0^2 = 4\,\mathrm{GeV}^2$)

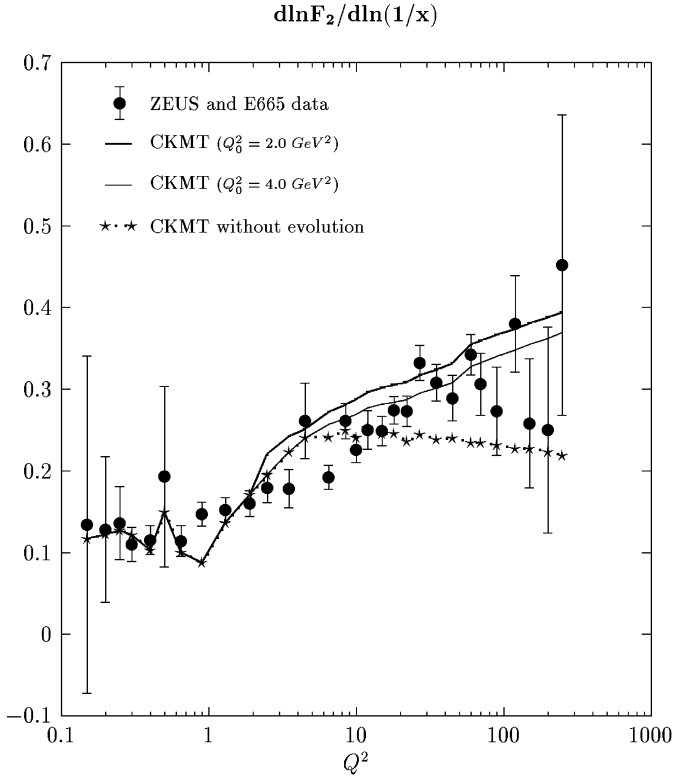

Fig. 4. $\mathrm{d}\ln F_2/\mathrm{d}\ln(1/x)$ as a function of Q^2 calculated by performing the NLO QCD evolution of the CKMT model, and compared to the fit $F_2 = Ax^{-\Delta_{\mathrm{eff}}}$ of the ZEUS [14] and the E665 [8] data with $x < 0.01$. For details on the CKMT calculation, see Appendices A and B. The dotted line is the theoretical result obtained with the pure CKMT model, and the bold (solid) line is the result obtained with the NLO QCD-evoluted CKMT model when one takes $Q_0^2 = 2\,\mathrm{GeV}^2$ ($Q_0^2 = 4\,\mathrm{GeV}^2$)

for example [17]). This question has been studied theoretically in [18,19]. Figure 3 shows that the CKMT model is in a good agreement with experimental points in the whole region of x and Q^2. One problem with the presentation of the data in Fig. 3 is a strong correlation between the x and Q^2 values for the data points. It follows from the formulas of the CKMT model for $\mathrm{d}F_2(x,Q^2)/\mathrm{d}\ln Q^2$ given in Appendix B that for a fixed value of Q^2 this quantity monotonically increases as $x \to 0$. The existence of a maximum of $\mathrm{d}F_2(x,Q^2)/\mathrm{d}\ln Q^2$ in Fig. 3 is related to the correlation between Q^2 and x in the region of small x (or Q^2). The same conclusion was reached in [18], and recently confirmed by experimental data [16].

Figures 4 and 5 show the slope $\mathrm{d}\ln F_2/\mathrm{d}\ln(1/x)$ as a function of Q^2 compared to the fits $F_2 = Ax^{-\Delta_{\mathrm{eff}}}$ of the ZEUS [14] and H1 [13] data, respectively. In Fig. 4, as the x range of the BPC95 data is restricted, also the E665 [8] data are taken into account. This slope is sometimes interpreted as the Δ_{eff} of the pomeron exchange, $\Delta_{\mathrm{eff}} = \mathrm{d}\ln F_2/\mathrm{d}\ln(1/x)$. Let us note that in our approach Δ_{eff} for $Q^2 > Q_0^2$ cannot be interpreted as an effective pomeron intercept, because the QCD evolution leads to a substantial increase of Δ_{eff} as Q^2 increases. On the other hand, this effect should decrease as $x \to 0$.

In the experimental fits, each Q^2 bin corresponds to an average value of x, $\langle x\rangle$, calculated from the mean value of $\ln(1/x)$ weighted by the statistical errors of the corresponding F_2 values in that bin. Even though we can proceed as in the experimental fits, and we get a very good agreement with the data, since the estimation of $\langle x\rangle$ is in some sense artificial and arbitrary, and it introduces unphysical wiggles when drawing one full line connecting the different bins, we made for all the Q^2 bins in these figures the choice of the smallest x in the data, instead of considering a different $\langle x\rangle$ for each Q^2. This choice is based on the fact that the ansatz $\Delta_{\mathrm{eff}} = \mathrm{d}\ln F_2/\mathrm{d}\ln(1/x)$ is actually valid for small x, and it results in a smooth curve except for the jump in the region around $Q^2 \sim 50\,\mathrm{GeV}^2$, where the evolution procedure changes (again, see Appendix A for more details).

Since the structure function F_2 in the region of low x is determined to a large extent by the gluon component, we present our prediction for the behavior of this gluon component. Thus, Fig. 6 shows the gluon density distribution as a function of Q^2 calculated by performing the NLO QCD evolution of the CKMT model, and its

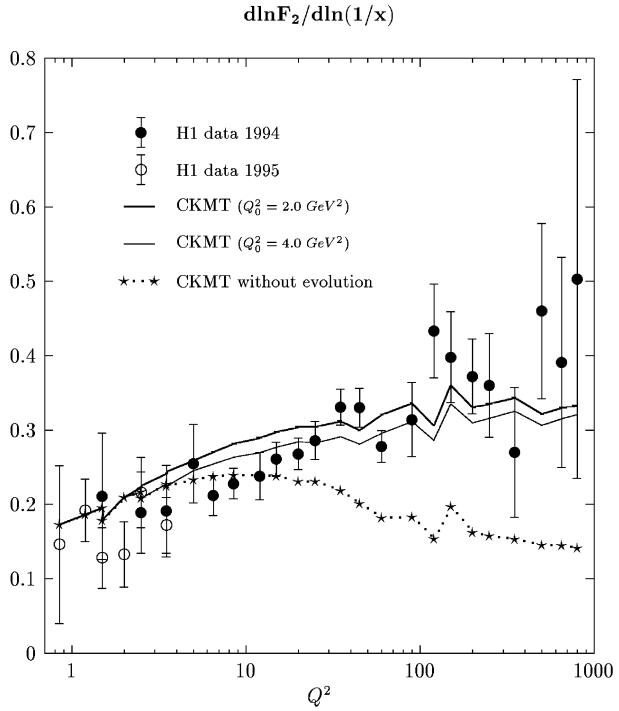

Fig. 5. $\mathrm{d}\ln F_2/\mathrm{d}\ln(1/x)$ as a function of Q^2 calculated by performing the NLO QCD evolution of the CKMT model, and compared to the fit $F_2 = Ax^{-\Delta_{\mathrm{eff}}}$ of the H1 data [13]. For details on the CKMT calculation, see appendices A and B. The dotted line is the theoretical result obtained with the pure CKMT model, and the bold (solid) line is the result obtained with the NLO QCD-evoluted CKMT model when one takes $Q_0^2 = 2\,\mathrm{GeV}^2$ ($Q_0^2 = 4\,\mathrm{GeV}^2$)

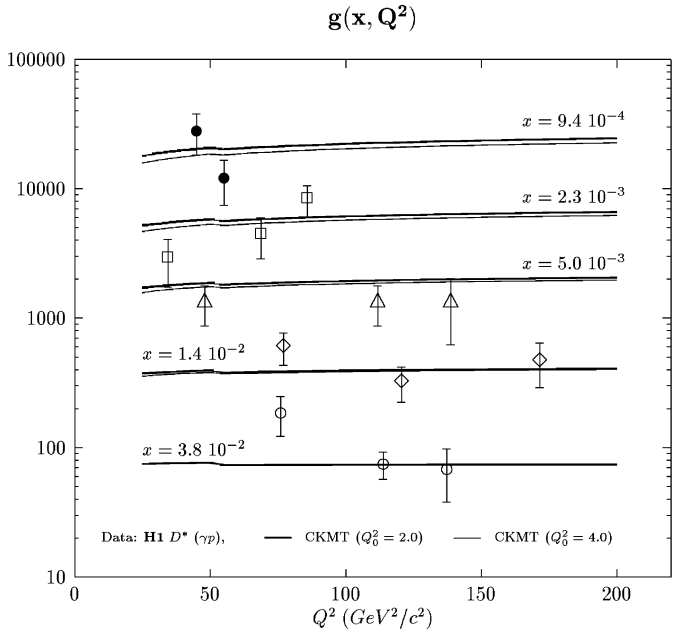

Fig. 6. Gluon density distribution as a function of Q^2 calculated by performing the NLO QCD evolution of the CKMT model, and compared with the H1 Collaboration data in [20]. We plot $g(x, Q^2)$ instead of $xg(x, Q^2)$, in order to show more clearly the evolution with the scale. In the theoretical calculation, the bold (solid) line has been obtained by taking a value of Q_0^2 of $Q_0^2 = 2\,\mathrm{GeV}^2$ ($Q_0^2 = 4\,\mathrm{GeV}^2$)

comparison with the H1 Collaboration data in [20]. Figure 7 represents the gluon densities at $\mu^2 = 25\,\mathrm{GeV}^2$ as a function of x calculated by evoluting the CKMT model at NLO, and compared to those determined from H1 DIS and photoproduction data. Experimental data on D^* meson cross-section measurements are from [16,20]. Figure 8 shows the behavior of $xg(x, \mu^2)$ at $\mu^2 = 200\,\mathrm{GeV}^2$ as a function of Q^2, to be compared with the H1-dijets results [16,21]. Finally, Fig. 9 shows the prediction of the CKMT model for $xg(x, Q^2)$ as a function of x at the values of Q^2 measured both by H1 and ZEUS collaborations.

A satisfactory agreement with the experiment is obtained in the whole ranges of x and Q^2 where experimental data are available. This shows that the experimental behavior of F_2, its logarithmic slopes, and its gluon component can be described by using as an initial condition for the QCD evolution equation a model of F_2 where the shadowing effects which are important at low values of Q^2 are included, like the CKMT model.

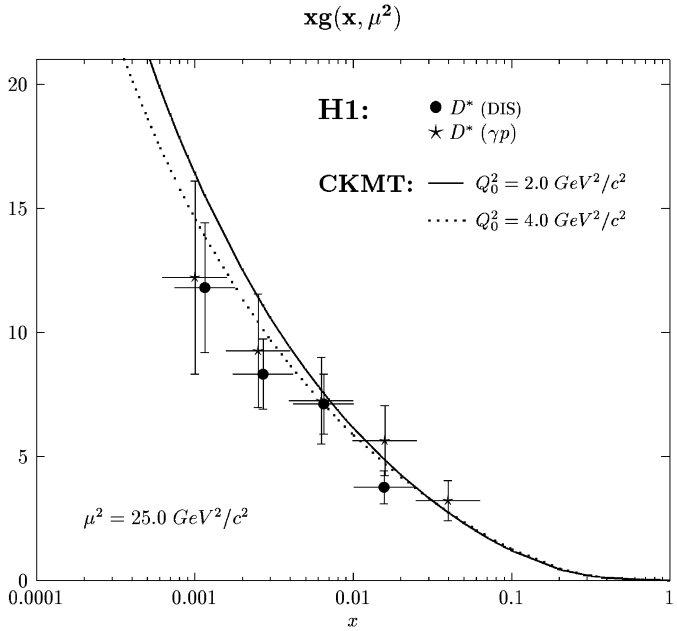

Fig. 7. Gluon densities at $\mu^2 = 25\,\mathrm{GeV}^2$ as a function of x, calculated by performing the NLO QCD evolution of the CKMT model, and compared to those determined from H1 DIS data (black dots), and from H1 photoproduction data (stars). Experimental data on D^* meson cross-section measurements are from [16,20]. In the theoretical calculation, the solid (dotted) line corresponds to a value of Q_0^2 at the starting point of the QCD evolution of $Q_0^2 = 2\,\mathrm{GeV}^2$ ($Q_0^2 = 4\,\mathrm{GeV}^2$)

3 Discussion and conclusions

Let us now compare the approach of the model considered in this paper [1] with other existing theoretical models for the description of the interaction of virtual photons with protons [18,19,22–28], both in the small and large

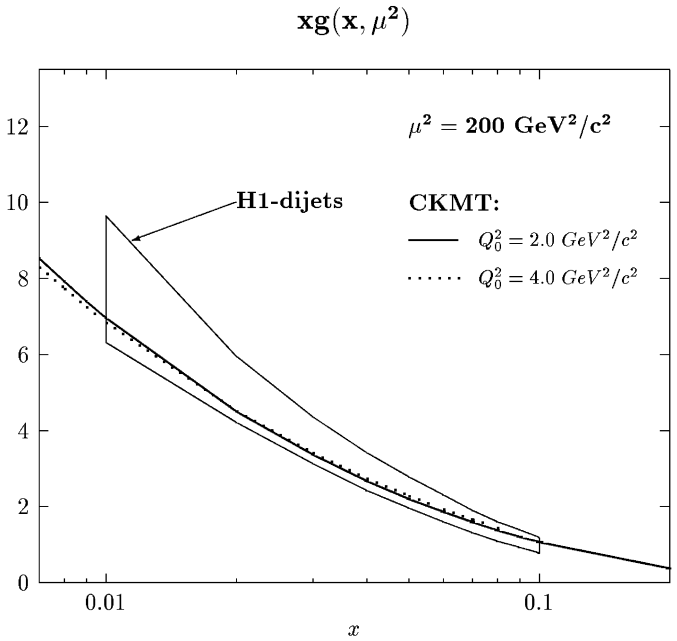

Fig. 8. Gluon density at $\mu^2 = 200\,\mathrm{GeV}^2$ as a function of x, calculated by performing the NLO QCD evolution of the CKMT model, to be compared with that obtained from the analysis of the H1 dijet data [16,21]. In the theoretical calculation, the solid (dotted) line has been obtained by taking a value of Q_0^2 at the starting point of the QCD evolution of $Q_0^2 = 2\,\mathrm{GeV}^2$ ($Q_0^2 = 4\,\mathrm{GeV}^2$)

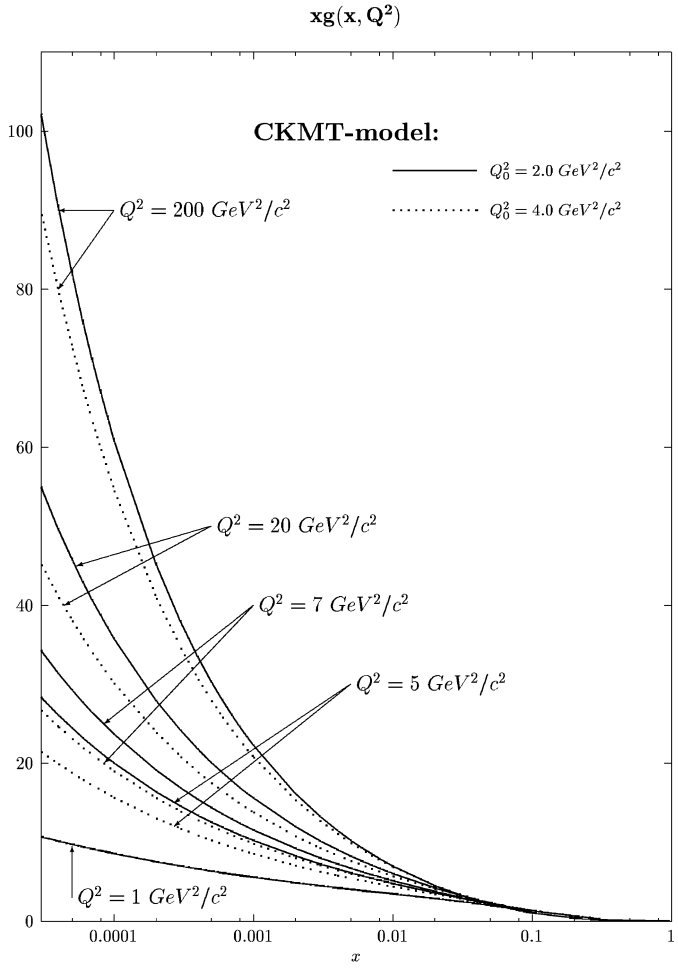

Fig. 9. Prediction of the behavior of $xg(x,Q^2)$ as a function of x, for several values of Q^2 measured by both H1 and ZEUS collaborations. The experimental points are not shown since the analysis of the more recent data is not completed. The solid (dotted) lines have been obtained by taking a value of Q_0^2 at the starting point of the QCD evolution of $Q_0^2 = 2\,\mathrm{GeV}^2$ ($Q_0^2 = 4\,\mathrm{GeV}^2$)

Q^2 regions. The ALLM parameterization [18] uses Q^2-dependent powers of $1/x$, but contrary to [1] it does not specify a dynamic origin of this dependence and it does not introduce QCD evolution. In [23,26,28] some forms of vector dominance are used to describe the dynamics in the low Q^2 region, while perturbative QCD calculations are applied at large Q^2. In [19], the dipole model of the pomeron is applied to a description of F_2 in a broad region of Q^2. The model of the BFKL pomeron with running coupling constant is used in [25]. A "soft" pomeron contribution is also needed in this model for the description of the experimental data. Models with two pomerons ("soft" and "hard") are developed in [24,27]. In [24], QCD evolution equations fix the Q^2 dependence of the residues. A particular realization of the idea in [1] on the influence of shadowing (or saturation) effects on the effective intercept of the pomeron was presented in [29]. Thus, there are different theoretical ideas on the origin of the Q^2-dependent intercept experimentally observed at HERA, which also lead to different consequences for the behavior of the structure functions in the region of small $x \sim 10^{-6}$–10^{-8}. In the models of [24,25,27], for example, the effective intercept should increase as energy (or $1/x$) increases, while in models leading to saturation the effective intercept should decrease as $x \to 0$. Crucial information on the behavior of the structure functions in the region of extremely small x, not accessible at HERA, will be available at LHC.

Finally, we conclude that the CKMT model for the parameterization of the nucleon structure functions provides a very good description of all the available experimental data on $F_2(x,Q^2)$ at low and moderate Q^2, including the recent small-x HERA points.

An important ingredient of the model is the dependence of an effective intercept of the pomeron on Q^2. It has recently been shown [22] that such a behavior is naturally reproduced in a broad class of models based on reggeon calculus, which describes simultaneously the structure function F_2 and the diffractive production by virtual photons.

Use of the CKMT model as the initial condition for the QCD evolution equations in the region of $Q^2 = 2$–$5\,\mathrm{GeV}^2$ leads to a good description of all available data in a broad region of Q^2, including the logarithmic slopes of the structure function $F_2(x,Q^2)$, $\mathrm{d}F_2(x,Q^2)/\mathrm{d}\ln Q^2$, and $\mathrm{d}\ln F_2(x,Q^2)/\mathrm{d}\ln(1/x)$. Thus, a unified description of the data on F_2 for all values of Q^2 is achieved.

Acknowledgements. A.B.K. acknowledges support by NATO grant OUTR.LG971390 and RFBR grant 98-02-17463, and C.M. was partially supported by CICYT (AEN99-0589-C02-02).

Appendix A: NLO QCD evolution of $F_2(x, Q^2)$

For the reader's convenience we present here some technical remarks concerning the NLO QCD calculation of $F_2(x, Q^2)$.

For sufficiently large $Q^2 > 1\,\mathrm{GeV}^2$, the structure function $F_2(x, Q^2)$ can be expressed by perturbative parton distributions. In leading order (LO) perturbation theory, the expression is given by

$$\frac{1}{x}F_2(x,Q^2) = x\sum_q e_q^2\{q(x,Q^2)+\bar{q}(x,Q^2)\}, \tag{12}$$

where q and $\bar{q}$ denote the quark and anti-quark distribution functions, e_q^2 is the squared quark electric charge, and the sum runs over all included quark flavors [11]. On the other hand, with $F_2(x, Q^2)$ given in (1)–(5), and making reasonable assumptions concerning the flavor structure of the QCD sea, one can extract from $F_2(x, Q^2)$ the different parton distribution functions, including that of the gluon component [1]. Generally, the calculation of $F_2(x, Q^2)$ at $Q^2 \gg 1\,\mathrm{GeV}^2$ requires a Q^2 evolution à la DGLAP [30]. The procedure consists in the solution of the LO-DGLAP equations for the parton distribution functions taking reasonable initial distributions at a starting value $Q^2 = Q_0^2$ ($1\,\mathrm{GeV}^2 < Q_0^2 < 5\,\mathrm{GeV}^2$). Using (12), the resulting quark distributions at Q^2 can be recombined to F_2 at this virtuality.

By the evolution of the CKMT model we mean the application of this procedure to the model discussed in this paper. As mentioned above, the CKMT model of $F_2(x, Q^2)$ is valid within $0 \le Q^2 < 5\,\mathrm{GeV}^2$. Due to the good agreement of the CKMT model with the experimental data in this region, the parton distributions extracted from F_2^{CKMT} at a Q_0^2 in that range seem to be reasonable initial distributions for the evolution to higher Q^2.

In next to leading order (NLO), the relation between $F_2(x, Q^2)$ and the parton distribution functions is more complicated and depends on the renormalization scheme. The calculations presented here are performed in the $\overline{\mathrm{MS}}$ scheme [31]. In this context, the structure function is given [11] by

$$\frac{1}{x}F_2(x,Q^2) = \sum_q e_q^2\Bigg\{q(x,Q^2)+\bar{q}(x,Q^2) + \frac{\alpha_s(Q^2)}{2\pi}\left[C_{q,2}*(q+\bar{q}) + 2\cdot C_{g,2}*g\right]\Bigg\}, \tag{13}$$

where $q, \bar{q}$ and g are the NLO quark, anti-quark and gluon distribution functions, respectively, and α_s denotes the strong coupling constant in NLO. The convolutions $C * q$ and $C * g$ are defined as

$$C*q = \int_x^1 \frac{\mathrm{d}y}{y} C\left(\frac{x}{y}\right) q(y,Q^2). \tag{14}$$

The Wilson coefficients $C_{q,g,2}(z)$ are given by

$$\begin{aligned} C_{q,2}(z) &= \frac{4}{3}\left[\frac{1+z^2}{1-z}\left(\ln\frac{1-z}{z}-\frac{3}{4}\right)+\frac{1}{4}(9+5z)\right]_+, \\ C_{g,2}(z) &= \frac{1}{2}\left[(z^2+(1-z)^2)\ln\frac{1-z}{z}-1+8z(1-z)\right]. \end{aligned} \tag{15}$$

Here, the integral over a $[\cdot]_+$-distribution is defined as described in [32]:

$$\begin{aligned} C_+ * q &= \int_x^1 \frac{\mathrm{d}y}{y} C\left(\frac{x}{y}\right)_+ q(y,Q^2) \\ &= \int_x^1 \frac{\mathrm{d}y}{y} C\left(\frac{x}{y}\right)\left[q(y,Q^2)-\frac{x}{y}q(x,Q^2)\right] \\ &\quad - q(x,Q^2)\int_0^x \mathrm{d}y C(y). \end{aligned} \tag{16}$$

There are alternative renormalization schemes as, for instance, the DIS scheme [11]. Here, the form of (12) is maintained at NLO, i.e.

$$\frac{1}{x}F_2(x,Q^2) = x\sum_q e_q^2\{q_{\mathrm{DIS}}(x,Q^2)+\bar{q}_{\mathrm{DIS}}(x,Q^2)\}. \tag{17}$$

The relation between the $\overline{\mathrm{MS}}$- and the DIS-distributions is given by

$$\begin{aligned} \overset{(-)}{q}{}_{\mathrm{DIS}}(x,Q^2) &= \overset{(-)}{q}(x,Q^2) \\ &\quad + \frac{\alpha_s(Q^2)}{2\pi}\left[C_{q,2}*\overset{(-)}{q}+C_{g,2}*g\right] + O(\alpha_s^2), \\ g_{\mathrm{DIS}}(x,Q^2) &= g(x,Q^2) \\ &\quad - \frac{\alpha_s(Q^2)}{2\pi}\left[\sum_q C_{q,2}*(q+\bar{q}) + 2f\cdot C_{g,2}*g\right] + O(\alpha_s^2). \end{aligned} \tag{18}$$

The parameter f denotes the number of active flavors in the sea.

Our procedure to extract the parton distributions from F_2^{CKMT} is based on the LO formula (12). Therefore, at NLO we extract the DIS-distributions. Now, the task is to calculate the $\overline{\mathrm{MS}}$-distributions at $Q^2 = Q_0^2$. This can be done by using a first order approximation in $\alpha_s(Q^2)/2\pi$:

$$\begin{aligned} \overset{(-)}{q}(x,Q_0^2) &\approx \overset{(-)}{q}{}_{\mathrm{DIS}}(x,Q_0^2) \\ &\quad - \frac{\alpha_s(Q_0^2)}{2\pi}\left[C_{q,2}*\overset{(-)}{q}{}_{\mathrm{DIS}}+C_{g,2}*g_{\mathrm{DIS}}\right], \\ g(x,Q_0^2) &\approx g_{\mathrm{DIS}}(x,Q_0^2) \\ &\quad + \frac{\alpha_s(Q_0^2)}{2\pi}\left[\sum_q C_{q,2}*(q_{\mathrm{DIS}}+\bar{q}_{\mathrm{DIS}}) + 2f\cdot C_{g,2}*g_{\mathrm{DIS}}\right]. \end{aligned} \tag{19}$$

In summary, the Q^2 evolution of F_2^{CKMT} works as follows:

(1) One chooses one appropriate value $Q^2 = Q_0^2 > 1\,\mathrm{GeV}^2$ as the starting point for the evolution. In our calculations, this value is $Q_0^2 = 2\,\mathrm{GeV}^2$ or $Q_0^2 = 4\,\mathrm{GeV}^2$.
(2) At $Q^2 = Q_0^2$, one extracts the NLO parton distribution functions from F_2^{CKMT}. The relation between these parton distributions and the structure function is given by (17), which is formally the same as (12) in LO, so the resulting parton distributions are the DIS-functions, i.e. $q_{\mathrm{DIS}}(x,Q_0^2), \bar{q}_{\mathrm{DIS}}(x,Q_0^2)$ and $g_{\mathrm{DIS}}(x,Q_0^2)$.
(3) Using (19) one calculates the $\overline{\mathrm{MS}}$-distributions $q(x, Q_0^2), \bar{q}(x,Q_0^2)$ and $g(x,Q_0^2)$.
(4) These $\overline{\mathrm{MS}}$-functions serve as initial distributions in a numerical procedure to solve the NLO-DGLAP equations in the $\overline{\mathrm{MS}}$ scheme for a certain value $Q^2 > Q_0^2$. The results are the evoluted $\overline{\mathrm{MS}}$ parton distributions $q(x,Q^2), \bar{q}(x,Q^2)$ and $g(x,Q^2)$.
(5) Finally, using (13), the structure function $F_2^{\mathrm{CKMT}}(x,Q^2)$ can be recalculated for any values of Q^2 and x.

Appendix B: The slopes of $F_2(x, Q^2)$

For low Q^2, the CKMT model is used as defined in (1)–(5). Here, the calculation of the logarithmic slopes $\mathrm{d}F_2(x,Q^2)/\mathrm{d}\ln Q^2$ and $\mathrm{d}\ln F_2(x,Q^2)/\mathrm{d}\ln(1/x) = \Delta_{\mathrm{eff}}$ is straightforward. Considering x and Q^2 as independent variables one gets

$$\begin{aligned}\frac{\mathrm{d}F_2(x,Q^2)}{\mathrm{d}\ln Q^2} &= F_{\mathrm{S}}(x,Q^2)\left[\frac{\Delta_2}{Q^2+\Delta_2}\left(\Delta(Q^2)-\Delta_0\right)\right.\\ &\times\ln\frac{Q^2}{x(Q^2+a)}+\frac{c}{Q^2+c}\left(n(Q^2)-\frac{3}{2}\right)\\ &\times\ln(1-x)+\left.\frac{a\left(1+\Delta(Q^2)\right)}{Q^2+a}\right]\\ &+F_{\mathrm{NS}}(x,Q^2)\left[\frac{c}{Q^2+c}\left(n(Q^2)-\frac{3}{2}\right)\right.\\ &\times\ln(1-x)+\left.\frac{b\alpha_{\mathrm{R}}(0)}{Q^2+b}\right], \end{aligned} \tag{20}$$

which in the limit $Q^2 \to 0$ takes the form

$$\begin{aligned}\frac{\mathrm{d}F_2(x,Q^2)}{\mathrm{d}\ln Q^2} &\sim (1+\Delta_0)\,F_{\mathrm{S}}(x,Q^2)\\ &+\alpha_{\mathrm{R}}(0)F_{\mathrm{NS}}(x,Q^2).\end{aligned} \tag{21}$$

Also, for the case when W is fixed one can take $x \sim C\cdot Q^2$, and then, up to constant factors, one gets

$$\begin{aligned}\frac{\mathrm{d}F_2(x,Q^2)}{\mathrm{d}\ln Q^2} &= F_{\mathrm{S}}(x,Q^2)\left[-\frac{\Delta_2}{Q^2+\Delta_2}\left(\Delta(Q^2)-\Delta_0\right)\right.\\ &\times\ln(Q^2+a)-\Delta(Q^2)+\frac{c}{Q^2+c}\\ &\times\left(n(Q^2)-\frac{3}{2}\right)\ln(1-Q^2)-\frac{Q^2n(Q^2)}{1-Q^2}\\ &+\left.\frac{a(1+\Delta(Q^2))}{Q^2+a}\right]+F_{\mathrm{NS}}(x,Q^2)\\ &\times\left[\frac{c}{Q^2+c}\left(n(Q^2)-\frac{3}{2}\right)\ln(1-Q^2)\right.\\ &+\left.\frac{b\alpha_{\mathrm{R}}(0)}{Q^2+b}+(1-\alpha_{\mathrm{R}}(0))-\frac{Q^2n(Q^2)}{1-Q^2}\right]. \end{aligned} \tag{22}$$

If now one takes W fixed with $Q^2 \sim x \to 0$, one can easily see that this equation simply reduces to

$$\frac{\mathrm{d}F_2(x,Q^2)}{\mathrm{d}\ln Q^2} \sim F_2(x,Q^2). \tag{23}$$

The calculations presented in this paper are based on the assumption of independent x and Q^2, i.e., (20) and (21). In this context, the effective x-slope, $\Delta_{\mathrm{eff}} = \mathrm{d}\ln F_2(x,Q^2)/\mathrm{d}\ln(1/x)$, is given by

$$\begin{aligned}&F_2(x,Q^2)\cdot\frac{\mathrm{d}\ln F_2(x,Q^2)}{\mathrm{d}\ln(1/x)}\\ &=\left[\Delta(Q^2)+\frac{x}{1-x}(n(Q^2)+4)\right]\cdot F_{\mathrm{S}}\\ &+\left[\alpha_{\mathrm{R}}(0)-1+\frac{x}{1-x}n(Q^2)+\frac{xB_d}{B_u+B_d(1-x)}\right]\cdot F_{\mathrm{NS}}.\end{aligned} \tag{24}$$

For $Q^2 > Q_0^2$, these logarithmic slopes have to be calculated from the evoluted structure function. Two different procedures are possible: pure numerical and mainly analytical calculations. The pure numerical procedure is very simple:

$$\begin{aligned}\frac{\mathrm{d}F_2(x,Q^2)}{\mathrm{d}\ln Q^2} &\approx Q^2\cdot\frac{1}{2\delta Q^2}\cdot\Big[F_2(x,Q^2+\delta Q^2)\\ &-F_2(x,Q^2-\delta Q^2)\Big],\end{aligned} \tag{25}$$

$$\begin{aligned}\frac{\mathrm{d}\ln F_2(x,Q^2)}{\mathrm{d}\ln(1/x)} &\approx(-1)\cdot\frac{x}{F_2(x,Q^2)}\cdot\frac{1}{2\delta x}\cdot\Big[F_2(x+\delta x,Q^2)\\ &-F_2(x-\delta x,Q^2)\Big].\end{aligned} \tag{26}$$

Here, $F_2(x,Q^2)$ is the evoluted structure function, whereas δQ^2 and δx denote the corresponding increments in Q^2 and x. These increments are fixed at $\delta Q^2 = 10^{-3}\cdot Q^2$ and $\delta x = 10^{-3}\cdot x$ in the present calculations. For low Q^2, we have checked this procedure comparing the values of (25) and (26) with those calculated using (20) and (24). The agreement is very good, getting, in some cases, identical numbers from both sets of equations. This numerical procedure is the method used to determine the effective x-slope, $\Delta_{\mathrm{eff}} = \mathrm{d}\ln F_2(x,Q^2)/\mathrm{d}\ln(1/x)$, of the evoluted structure function. In the case of $\mathrm{d}F_2(x,Q^2)/\mathrm{d}\ln Q^2$ also mainly analytical calculations are possible. If the parton distribution functions are known, their derivatives concerning Q^2 can be calculated from the DGLAP equations. Instead of Q^2, the parameter S,

$$S=\ln\left\{\frac{T}{T_\circ}\right\},\quad T=\ln(Q^2/\Lambda^2_{\mathrm{QCD}}),\quad T_\circ=\ln(Q_0^2/\Lambda^2_{\mathrm{QCD}}), \tag{27}$$

is often used in perturbation theory. In terms of S

$$\frac{\mathrm{d}F_2}{\mathrm{d}\ln Q^2} = \frac{1}{\ln(Q^2/\Lambda^2_{\mathrm{QCD}})}\frac{\mathrm{d}F_2}{\mathrm{d}S}, \tag{28}$$

and, in the $\overline{\mathrm{MS}}$ scheme,

$$\begin{aligned}\frac{1}{x}\frac{\mathrm{d}F_2(x,S)}{\mathrm{d}S} &= \sum_q e_q^2 \left\{ \frac{\mathrm{d}q(x,S)}{\mathrm{d}S} + \frac{\mathrm{d}\bar{q}(x,S)}{\mathrm{d}S} \right. \\ &+ \frac{\alpha_{\mathrm{s}}(Q^2)}{2\pi}\left[C_{q,2} * \left(\frac{\mathrm{d}q}{\mathrm{d}S} + \frac{\mathrm{d}\bar{q}}{\mathrm{d}S}\right) + 2\cdot C_{g,2} * \frac{\mathrm{d}g}{\mathrm{d}S}\right] \\ &\left. + \frac{1}{2\pi}\frac{\mathrm{d}\alpha_{\mathrm{s}}(Q^2)}{\mathrm{d}S}\left[C_{q,2} * (q+\bar{q}) + 2\cdot C_{g,2} * g\right]\right\}. \end{aligned} \tag{29}$$

The numerical integration procedure for solving the DGLAP equations we have used gives the evoluted parton distributions and their derivatives on S as output. In NLO, $\mathrm{d}\alpha_{\mathrm{s}}(Q^2)/\mathrm{d}S$ is simple to calculate:

$$\begin{aligned}\frac{\alpha_{\mathrm{s}}(T)}{2\pi} &= \frac{2}{\beta_0 T}\left(1 - \frac{\beta_1}{\beta_0^2}\frac{\ln(T)}{T}\right), \\ \frac{1}{2\pi}\frac{\mathrm{d}\alpha_{\mathrm{s}}(T)}{\mathrm{d}T} &= -\frac{1}{T}\cdot\frac{\alpha_{\mathrm{s}}(T)}{2\pi} + \frac{2\beta_1}{\beta_0^2 T^3}(\ln(T)-1), \\ \frac{1}{2\pi}\frac{\mathrm{d}\alpha_{\mathrm{s}}}{\mathrm{d}S} &= T\cdot\frac{1}{2\pi}\frac{\mathrm{d}\alpha_{\mathrm{s}}}{\mathrm{d}T}. \end{aligned} \tag{30}$$

Thus, with the derivatives $\mathrm{d}q/\mathrm{d}S$, $\mathrm{d}\bar{q}/\mathrm{d}S$ and $\mathrm{d}g/\mathrm{d}S$, one gets the Q^2-derivative of F_2. This method is called mainly analytical (it still includes a numerical integration procedure).

Equation (29) is valid [11,12] for $Q^2 > Q_0^2$. As described in the main text, charm is treated via a photon–gluon fusion process in the range $Q_c^2 < Q^2 < \bar{Q}^2 = 50\,\mathrm{GeV}^2$ [11,12]. From (9), the charm slope contribution can be determined to be

$$\begin{aligned}\frac{1}{x}\frac{\mathrm{d}F_2^c(x,Q^2,m_c^2)}{\mathrm{d}\ln Q^2} &= 2e_c^2\frac{\alpha_{\mathrm{s}}(\mu^2)}{2\pi}\int_{ax}^1 \frac{\mathrm{d}y}{y}\cdot\frac{\mathrm{d}C_{g,2}^c}{\mathrm{d}\ln Q^2} \\ &\times\left(\frac{x}{y},\frac{m_c^2}{Q^2}\right)\cdot g(y,\mu^2). \end{aligned} \tag{31}$$

The total slope is the sum of (29) and (31).

We have calculated the Q^2-slope of the evoluted F_2 in the perturbative region $Q^2 \geq Q_0^2$, using both the numerical and the analytical methods. The values obtained in both procedures are in agreement, although the differences somewhat increase in the region near Q_0^2. The values in the presented figures are from the numerical calculation.

References

1. A. Capella, A.B. Kaidalov, C. Merino, J. Tran Than Van, Phys. Lett. B **337**, 358 (1994)
2. A.B. Kaidalov, Z. Phys. C **12**, 63 (1982); Phys. Lett. B **116**, 459 (1982); A.B. Kaidalov, K.A. Ter-Martirosyan, Phys. Lett. B **117**, 247 (1982)
3. A. Capella, U. Sukhatme, C.-I. Tan, J. Tran Than Van, Phys. Rep. **236**, 225 (1994)
4. P. Amaudruz et al. (New Muon Collaboration), Phys. Lett. B **259**, 159 (1992)
5. C. Adloff et al. (H1 Collaboration), Nucl. Phys. B **497**, 3 (1997)
6. J. Breitweg et al. (ZEUS Collaboration), Phys. Lett. B **407**, 432 (1997)
7. A.B. Kaidalov, C. Merino, hep-ph/9806367; Eur. Phys. J. C **10**, 153 (1999)
8. M.R. Adams et al. (E665 Collaboration), FERMILAB-Pub 1995/396; Phys. Rev. D **54**, 3006 (1996)
9. D.O. Caldwell et al., Phys. Rev. Lett. **40**, 1222 (1978); M. Derrick et al. (ZEUS Collaboration), Phys. Lett. B **293**, 465 (1992); Z. Phys. C **63**, 391 (1994); S. Aid et al. (H1 Collaboration), Z. Phys. C **69**, 27 (1995)
10. F. Martin, Phys. Rev. D **19**, 1382 (179)
11. M. Glück, E. Reya, A. Vogt, Z. Phys. C **67**, 433 (1995)
12. L.P.A. Haakman, A.B. Kaidalov, J.H. Koch, hep-ph/9704203; Eur. Phys. J. C **1**, 547 (1999)
13. S. Aid et al. (H1 Collaboration), DESY-96-039, hep-ex/9603004, contribution to the Proceedings of the XXXI Rencontres de Moriond: QCD and High Energy Hadronic Interactions, Les Arcs (France), March 1996, edited by J. Tran Thanh Van (Editions Frontières, Gif-sur-Yvette, France 1996), pp. 349–355; Nucl. Phys. B **470**, 3 (1996)
14. A. Caldwell, DESY Theory Workshop, DESY, Hamburg (Germany), October 1997; J. Breitweg et al. (ZEUS Collaboration), DESY-98-121, hep-ex/9809005; Eur. Phys. J. C **7**, 609 (1999)
15. C. Amelung (ZEUS Collaboration), contribution to the Proceedings of the 7th International Workshop on Deep Inelastic Scattering and QCD (DIS99), DESY Zeuthen, Germany, April 19–23 1999, edited by J. Blümlein, T. Riemann, Nucl. Phys. B Proc. **79**, 176 (1999)
16. A. Zhokin, on behalf of the H1 and ZEUS collaborations, contribution to the Proceedings of the XXIX International Symposium on Multiparticle Dynamics (ISMD99), Brown University, Providence, RI 02912, USA, August 9–13 1999, edited by I. Sarcevic, C.-I. Tang (World Scientific), pp. 71–78
17. A.H. Mueller, contribution to the Proceedings of the 6th International Workshop on Deep Inelastic Scattering and QCD (DIS98), Brussels, Belgium, April 4–8 1998, edited by Gh. Coremans, R. Roosen (World Scientific), pp. 3–19
18. E. Gotsman, E. Levin, U. Maor, Nucl. Phys. B **425**, 369 (1998); **539**, 535 (1999); H. Abramowicz, A. Levy, E. Levin, U. Maor, Phys. Lett. B **269**, 465 (1991); H. Abramowicz, A. Levy, hep-ph/9712415
19. P. Desgrolard, L.L. Jenkovszky, A. Lengyel, F. Paccanoni, hep-ph/9903397; Phys. Lett. B **459**, 265 (1999); P. Desgrolard, A. Lengyel, E. Martynov, Phys. Lett. B **437**, 408 (1998); Eur. Phys. J. C **7**, 665 (1999)
20. C. Adloff et al. (H1 Collaboration), Nucl. Phys. B **545**, 21 (1999)
21. M. Wobisch (H1 Collaboration), Proceedings of the 7th International Workshop on Deep Inelastic Scattering and QCD (DIS99), DESY Zeuthen, Germany, April 19–23 1999, edited by J. Blümlein, T. Riemann, Nucl. Phys. B Proc. **79**, 478 (1999)
22. A. Capella, E.G. Ferreiro, A.B. Kaidalov, C.A. Salgado, hep-ph/0005049; hep-ph/0006233

23. B. Badelek, J. Kwiecinski, Phys. Lett. B **295**, 263 (1992); Rev. Mod. Phys. **68**, 445 (1996)
24. C. López, F. Barreiro, F.J. Ynduráin, Z. Phys. C **72**, 561 (1996); K. Adel, F. Barreiro, F.J. Ynduráin, Nucl. Phys. B **495**, 221 (1997)
25. N.N. Nikolaev, B.G. Zakharov, V.R. Zoller, JETP Lett. **66**, 103 (1997); N.N. Nikolaev, V.R. Zoller, JETP Lett. **69**, 103 (1999); **69**, 187 (1999)
26. D. Schildknecht, Act. Phys. Polon. B **28**, 2453 (1997); hep-ph/0006153
27. A. Donnachie, P.V. Landshoff, Phys. Lett. B **437**, 408 (1998)
28. A.D. Martin, M.G. Ryskin, A. Stasto, Eur. Phys. J. C **7**, 643 (1999)
29. K. Golec-Biernat, M. Wusthoff, Phys. Rev. D **59**, 014017 (1999)
30. Yu.L. Dokshitzer, JETP Lett. **46**, 641 (1977); V.N. Gribov, L.N. Lipatov, Sov. J. Nucl. Phys. **15**, 438 (1972); G. Altarelli, G. Parisi, Nucl. Phys. B **126**, 298 (1977)
31. W.A. Bardeen, A.J. Buras, D.W. Duke, T. Muta, Phys. Rev. D **18**, 3998 (1978)
32. M. Glück, E. Reya, A. Vogt, Z. Phys. C **63**, 127 (1992)